Water Distribution Systems

F.A. Bombardelli

Department of Civil and Environmental Engineering

University of California

Davis, CA 95616

INTRODUCTION

Water resources have been essential in the development of Mankind and play a fundamental role in the way people relate to the environment. At the individual level, humans need drinking water for daily survival. Water regulates physical and biochemical processes within the human body, ranging from the digestion of food and the control of the body temperature, to the elimination of body wastes. Modern life in the developed world takes for granted the availability of water for basic uses such as drinking, cleaning and cooking. Water courses and water bodies are also exploited for power generation, recreation, irrigation, etc.

Communities have historically developed in close proximity to water courses and water bodies. Numerous examples across diverse continents include early villages of Mesopotamia (near the Euphrates and Tigris Rivers), Egypt (in the valley of the Nile River), and Crete (Mays 2007, 2008). Nearby water courses allowed members of the community to obtain fresh water for basic uses, and to discharge their wastes. When communities were of relatively small size, their impact on the environment was relatively low. However, with the historical growth of population and the development of more formal settlements, a strong need for large-scale

infrastructure arose. Hydraulic structures were needed to collect water from neighboring water bodies, store it, and distribute it over large distances. According to Mays (2007), rivers and springs were both exploited in ancient Greece, and hydraulic structures such as wells, cisterns, and aqueducts were constructed during the Minoan culture, circa 2900-2300 B.C. Cisterns were sometimes built to store rainfall collected from roofs and courtyards. The city of Tylissos of the Minoan era was built with an aqueduct made of pipes and stone channels, and a sediment tank. Today, it is possible to see relics of these structures (Mays 2007). Figure 1 shows portions of the water system in Tylissos. These hydraulic structures can be considered as sample components of what it is known today as water supply systems (WSSs) and water distribution systems (WDSs). One of the milestones in the development of ancient WDSs is the tunnel of Eupalinos on Samos Island, built by the Greek circa 530 B.C., the first deep tunnel in history whose construction started from two different openings (Mays 2008). Aqueducts and terracotta pipes became common infrastructure of Greek cities, indicating that water supply was an essential aspect of the welfare of those communities. Greek water systems also used inverted siphons, lead pipes to withstand larger pressures and, for the first time, Archimedes screws (Archimedes, 287-212 B.C.) and "force pumps" (Mays 2008).

The Romans developed technology to obtain water not only from wells and springs, but also by damming rivers. Large aqueducts were part of massive supply systems built by the Romans, and many of them can still be seen in Spain, France, Rome, and North Africa (Mays 2008; Chanson 2002). Romans built tapped water storage tanks called *castella* that served multiple groups of people at once. The city of Pompeii (located in the Bay of Naples, Italy) developed a WDS that followed a typical Roman design, with pipes to supply water to a few private baths (Mays 2008). Romans also developed diverse types of valves and pumps (Mays

2008). Another major contribution of Romans to the water supply of cities was the development of drop shafts within aqueducts. These structures served for several purposes: (1) accommodating sharp drops in topography; (2) dissipating kinetic energy; and (3) aerating the flow (Chanson 2002).

Figure 1. Images of relics of the water system in Tylissos, in ancient Crete. (a) Aqueduct to transport water from springs. (b) Sedimentation deposit (in foreground) with stone channel connecting to cistern (photos copyright by L.W. Mays).

Figure 2 shows a schematic of water supply and wastewater management systems in a generic, modern city. The left portion of the schematic shows the extraction of water from the river (by an unspecified method in the diagram), as well as from a reservoir, and wells. Water obtained from these sources is transported to a water treatment plant and then pumped towards houses and industries. Historically, WDSs have been associated (in a restricted sense) only with the set of hydraulic structures (mostly tanks and pipes) that convey water to houses and industries. According to this notion, a WDS is composed mainly by pressurized flows. Mays (2004) states that WDSs possess three main components: pumping systems, storage and distribution piping. It is possible to add to the description of WDSs discussed above the structures that extract water from rivers, reservoirs and wells, and the water treatment plant, obtaining a more general definition of WDSs. Therefore, in this chapter, WDSs are understood

in a general sense as a set of canals, pipes, water tower/s and other hydraulic structures designed to provide water to urban areas, *from the source to the consumer*, be it for domestic or industrial use.

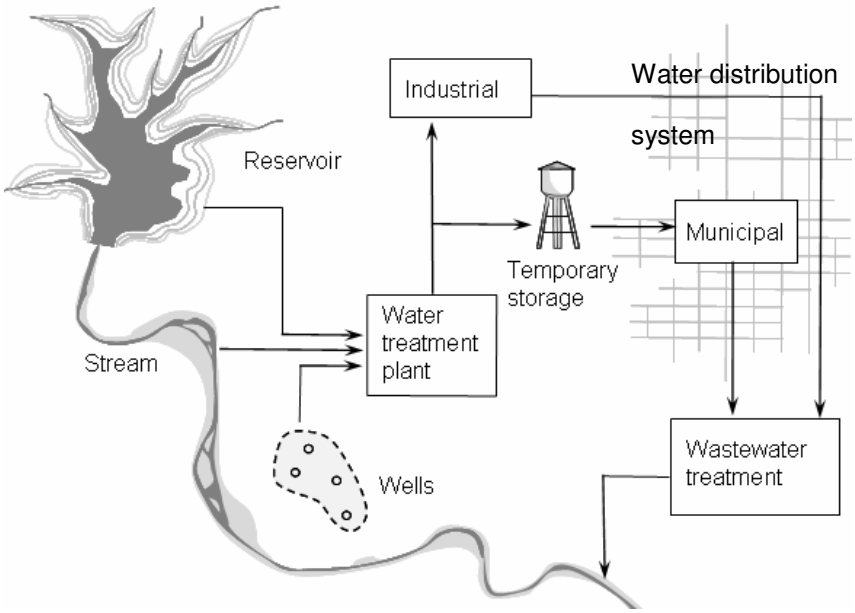

Figure 2. Schematic of water supply, distribution, and wastewater management systems in a modern city. Adapted from Masters (1997) and Mays (2004).

In some instances the WDS may cover an area a few kilometers across (say, less than 25 km), while in other situations the pipes, channels, pumping systems, storing tanks and other structures may cover hundreds of kilometers. Such is the case of the WDS for the Los Angeles area, in California. Water is "exported" south from the lower portion of the Sacramento-San Joaquin Delta (located in the Central Valley of the state), by a large pumping system. The water transport system is composed of an approximately 500 km-long aqueduct that includes several pumping stations along the way. Figure 3 shows diverse portions of channels, pipes and pumping systems for the WDS of the Los Angeles area.

Figure 3. Picture of the water supply system of the Los Angeles area. (a) California aqueduct (used with permission under the GNU project); (b) San Luis reservoir (http://www.water.ca.gov/swp); (c) Pyramid Lake (http://www.water.ca.gov/swp); (d) Edmonston pumping plant (http://www.water.ca.gov/swp).

A common feature of all hydraulic structures of WDSs is the presence of water flows of *turbulent nature*, which overcome the resistance to flow produced by solid boundaries. Most of these flows can be classified as shear flows, where the velocity is essentially one dimensional, but varies in space in a direction normal to the main direction of motion. Shear flows include wakes, boundary layers, submerged jets, open-channel and pipe flows, etc. (Davidson 2005). This chapter reviews the knowledge required to design hydraulic structures in WDSs, with an emphasis on the quantification of the resistance to flow. It also presents recent theoretical results which connect traditional design formulations to modern analyses of turbulence. These ideas are considered to be very important in everyday engineering as well as in research. The chapter aims at bridging the gap between practitioners and scientists.

II. PRINCIPLES AND METHODS OF ANALYSIS

Current knowledge and understanding of resistance to flow in pipes and open channels is the result of contributions by many scientists and engineers over the last three centuries. These contributions can be broadly classified as coming from the classic field of hydraulics (essentially during the 1700s and 1800s; Dooge 1992), and those coming from the traditional fluid mechanics field (1800s and 1900s; Kundu and Cohen 2008). It is interesting to note that the empirical contributions by engineers in the field of hydraulics were made prior to the seminal experiments of Reynolds in 1883 (O. Reynolds, 1842-1912), who addressed the existence of two main flow regimes: laminar and turbulent (Pope 2000, page 5).

II.1 Empirical equations for the quantification of flow resistance

Early systematic developments regarding flow in pipes and open channels were based mainly on empiricism. The equations most widely used to predict the cross-sectionally averaged flow velocity (U) in open channels and pipes include (Yen 1992a, 1992b, 2002; Bombardelli and García 2003):

- Manning's equation (R. Manning, 1830-1920)

$$U = \frac{K_n \, R_h^{2/3} \, S^{1/2}}{n} \qquad (1)$$

- Dimensionally homogeneous Manning formula (Yen 1992b; B. C. Yen, 1935-2001)

$$U = \frac{g^{1/2} \, R_h^{2/3} \, S^{1/2}}{n_g} \qquad (2)$$

- Chèzy's equation (A. de Chèzy, 1718-1798)

$$U = C \, R_h^{1/2} \, S^{1/2} \qquad (3)$$

- Darcy-Weisbach equation (H. Darcy, 1803-1858; J. Weisbach, 1806-1871)

$$U = \left(\frac{2\ g}{f} \right)^{1/2} \ D^{1/2} \left(\frac{h_f}{\Delta L} \right)^{1/2} \qquad (4)$$

- Hazen-Williams equation

$$U = K_{HW}\ C_{HW}\ R_h^{0.63}\ S^{0.54} \qquad (5)$$

where R_h is the hydraulic radius (i.e., the ratio between the wetted area and the wetted perimeter; Chow 1959), S denotes the slope of the energy grade line, D indicates the pipe diameter, ΔL refers to the length of the pipe segment, h_f is the energy loss in the pipe segment (expressed per unit weight of fluid), g is the acceleration of gravity, K_n and K_{HW} are both unit conversion factors, and n, n_g, C, f and C_{HW} indicate the *resistance/conveyance coefficients*. K_n is 1 $m^{1/2}/s$ in the International System (SI) or 1.486 $ft^{1/3}$-$m^{1/6}/s$ in English units. Using either system, Manning's *n* should have units of $m^{1/6}$ (Yen 1992b, 2002). K_{HW} equals 0.849 and 1.318 for the SI and English units, respectively (Jeppson 1977).

It is well known that the Darcy-Weisbach and Manning formulas can both be used for computations in either open-channel or pipe, fully-rough turbulent flow, provided the equivalence $D = 4\ R_h$ (for a circular pipe) is considered, and reliable estimates for the resistance coefficients are available (Yen 1992a, 2002; Bombardelli and García 2003). (Fully-rough flow is defined as the flow regime in which the roughness of the boundary controls the flow behavior; see Section II.2.1.) The Chèzy equation can also be employed in either case, also for turbulent, fully-rough flow. Based on these ideas, it is possible to state the following equivalence (Yen 1992a, 2002; Bombardelli and García 2003):

$$\sqrt{\frac{8}{f}} = \frac{C}{\sqrt{g}} = \frac{K_n\ R^{1/6}}{\sqrt{g}\ n} = \frac{R^{1/6}}{n_g} = \frac{U}{\sqrt{g\ R\ S}} = \frac{U}{u_*} \qquad (6)$$

with u_* indicating the wall-friction (shear) velocity, defined as the square root of the ratio between the shear stress at the wall and the fluid density.

The Hazen-Williams formula, in turn, has quite a restricted range of application that is often overlooked in practice. Diskin (1960) determined the ranges of Reynolds numbers, Re (i.e., the product of the flow velocity, U, and a flow length scale, L, divided by the kinematic viscosity of the fluid, v) for which the Hazen-Williams formula is applicable, concluding that the expression is *not* valid for fully-rough flow. In practical terms, Diskin also found that the use of the formula, when applied in the appropriate range, should result in values of C_{HW} between 100 and 160 (see also Bombardelli and García 2003).

Although many engineers and scientists tend to regard the Darcy-Weisbach formula as "more rationally based than other empirical exponential formulations" (Streeter et al. 1998), such an idea is somewhat misleading. In fact, all expressions can be obtained from dimensional analysis and in the end experiments are required to measure the resistance coefficients (Yen 1992a, 2002; Gioia and Bombardelli 2002).

Example 1 (on the use of the flow resistance equations): Compute the discharge (the volumetric flow rate) in an open channel of rectangular cross section, with a width of 2.5 m, and a slope of 0.002, for a water depth of 1.193 m, and $n = 0.012$ m$^{1/6}$.

Knowing n, and calculating the hydraulic radius ($R_h = 0.61$ m), it is possible to obtain all coefficients from Equation (6), as follows: $C = 76.7$ m$^{1/2}$/s, $f = 0.0133$. The velocity can then be obtained from (1) to (5), being equal to 2.68 m/s; the discharge is 8 m^3/s.

II.2 The semi-logarithmic law for flow velocities close to walls, and friction laws for turbulent flow in pipes and open channels

II.2.1 Flow regimes in pipes and open channels

Every solid boundary presents a certain degree of roughness, even those that seem smooth to the touch. From a fluid mechanics standpoint, this roughness exists as protrusions or indentations of the solid boundary acting on the flow, and imposing a drag on it. The drag on the flow will depend on the density, distribution, and size of the roughness elements on the surface of the pipe or channel walls (Schlichting 1968). Although the roughness elements are in reality non-uniform in size and location, it is customary to use a unique length scale, k, to represent such roughness. It is certainly remarkable that a relatively small length scale, when compared to other scales in the flow, can play such a tremendous role in defining the flow features close to solid walls under certain flow conditions (Gioia and Bombardelli 2002).

Experiments performed in the 1920s on pipes and open channels under *turbulent* flow conditions allowed for the identification of three main types of flow responses to the roughness elements (Schlichting 1968). In the first one, which occurs for instance in cement channels or cast iron pipes, the resistance to the flow only depends on the *relative roughness*, k/L_R, with L_R denoting either the pipe diameter or the hydraulic radius in open-channel flow. This regime is called *turbulent, fully-rough flow*. The second type of response occurs when the protrusions are relatively smaller, or are distributed over larger wall areas, as is the case of the flow in wooden or commercial steel pipes (Schlichting 1968). Under this condition, *both* k/L_R and the Reynolds number characterize the level of the resistance to flow. This regime is called *transitional flow*. The third type of flow is the *smooth regime*, where the flow resistance is dictated solely by the Reynolds number, in a similar fashion to what occurs in the Hagen-Poiseuille (laminar) pipe

flow (Schlichting 1968, page 80).

It turns out that for the same relative roughness, k/L_R, the flow behavior could vary from one regime to another depending on the flow condition. A dimensionless parameter is used to indicate the different flow regimes, obtained by dividing the roughness height, k, with a *viscous length scale*, ν/u_*, the ratio of the kinematic viscosity of water, ν, and the wall-friction (shear) velocity, u_*; i.e., $k\,u_*/\nu$. The different regimes are delimited as follows (Schlichting 1968):

Smooth regime	Transitional regime	Fully-rough regime
$0 \le \frac{k\,u_*}{\nu} < 5$ (7)	$5 \le \frac{k\,u_*}{\nu} \le 70$ (8)	$\frac{k\,u_*}{\nu} > 70$ (9)

The viscous length scale also defines the size of the *viscous sub-layer*, δ_v, a very thin region close to the wall where viscosity dominates over inertial forces. It must be emphasized that the flow in this region is indeed *turbulent*; not laminar as stated in old books on fluid mechanics (see Davidson 2005, page 130). Experimental results by Nikuradse (J. Nikuradse, 1894-1979) found that the viscous sub-layer can be computed as $\delta_v = 11.6\,\nu/u_*$. The explanation for the different flow regimes (embedded in Equations (7) to (9)) indicates that when the flow is smooth, the viscous sub-layer, δ_v, is larger than k, while it is smaller than k for fully-rough flow. However, this explanation has been challenged recently, and is further discussed in Section III.2.

There have been attempts to link the values of the resistance/conveyance coefficients with the roughness height values, mainly Manning's n. One such relationship was developed in 1923 by Strickler (Strickler 1981; A. Strickler, 1887-1963), as follows:

$$n = \frac{k^{1/6}}{21.1} \qquad (10)$$

with $k=d_{50}$ computed in meters. Very recently, Travis and Mays (2008) presented an expression connecting the Hazen-Williams C_{HW} with k:

$$k = D\left(3.32 - 0.021\, C_{HW}\; D^{0.01}\right)^{2.173}\; e^{-0.04125\, C_{HW}\; D^{0.01}} \qquad (11)$$

II.2.2 Velocity distribution in pipes and open channels and expressions for the friction factor

It took natural philosophers many centuries to realize that the flow velocity vector at a stationary and impervious wall, right at the wall, was zero. This condition is known today as the *no-slip and impermeability* conditions (Pope 2000, page 17). It also took the efforts of many researchers to address the nature and features of the velocity distribution close to a solid wall as a function of the distance from the wall. *The flow sufficiently close to solid boundaries at large Reynolds numbers is very similar for channels, pipes, and flat-plate boundary layers* in a region where the flow is statistically stationary and does not vary with the coordinate in the direction of motion. This region is called the *fully-developed* flow region.

The total shear stress (τ) within the fluid at a given distance z from the wall is the result of stresses coming from molecular origin (the viscous stresses), and the Reynolds stresses ($-\rho\,\overline{u'\,w'}$) which arise as a consequence of turbulence (Pope 2000). In this expression for the Reynolds stresses, u' and w' indicate the velocity fluctuations in x and z, respectively, ρ is the density of water, and the overbar indicates average over turbulence. At the wall, the Reynolds stresses are zero, because of the no-slip and impermeability conditions (Pope 2000). Therefore, the contribution from viscosity is the only stress remaining for the total shear stress at the wall (τ_w):

$$\tau_w \equiv \rho\,\nu\left(\frac{d\,\bar{u}}{d\,z}\right)_{z=0} \qquad (12)$$

Away from the wall, turbulent (Reynolds) stresses become prevalent, and the viscous stresses decay accordingly.

Immediately close to the wall, where viscosity dominates, the distances are better

described in viscous coordinates -- also called “wall units:”

$$z^+ \equiv \frac{z\, u_*}{\nu} \qquad (13)$$

where ν/u_* is the viscous length scale defined in the previous section. Far from the wall, $\eta = z/\delta$ provides a better scaling of distances. Here, δ is a measure of the boundary-layer thickness, given by the pipe radius in pipe flow (Schlichting 1968). The distance from the wall relative to the viscous length scale, i.e. z^+, and η help identifying different regions of flow behavior close to the wall. First, there is a consensus among researchers that there is a *viscous wall region* for $z^+ <$ 50, where viscosity significantly affects the shear stress, and an *outer layer* for $z^+ > 50$, where viscosity effects are negligible. Some researchers have also suggested the existence of sub-regions within the above two main regions (Pope 2000; Jiménez 2004). The viscous sub-layer holds for $z^+ < 5$, and there is an *inner layer* which reaches up to $z^+ = 1{,}000$ or up to $\eta = 0.1$. This indicates that there is an *overlap region* of the inner and outer layers from $z^+ = 50$ to 1,000 (see Figure 4(a)).

(a) (b)

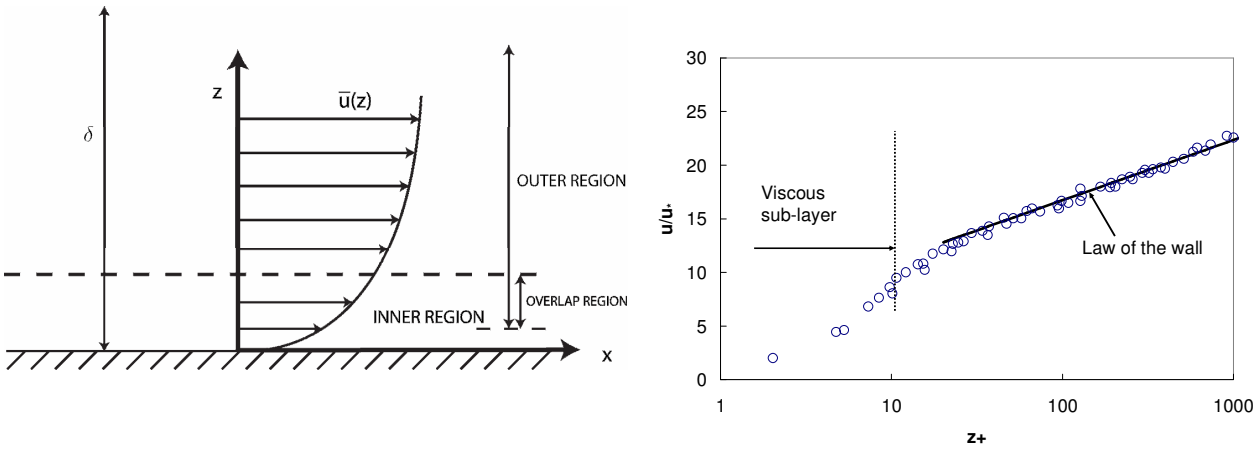

Figure 4. (a) Schematic of the regions close to a wall (adapted from Davidson 2005, page 128). (b) Comparison of time-averaged velocity data for fully-developed, turbulent channel flow (compiled by Pope) with the law of the wall. Data pertains to Reynolds numbers ranging from 2,970 to 39,582 (adapted from Pope 2000, page 275).

When concerned with the time-averaged velocity distribution in the fully-developed flow region, the important variables are: the water density, ρ, the kinematic viscosity of water, ν, the wall-friction (shear) velocity, u_*, and the thickness of the boundary layer, δ. Using dimensionless numbers, the above variables result in (Pope 2000):

$$\bar{u}(z) = u_* \; F(\frac{z}{\delta}, \text{Re}) \quad (14a)$$

where *F(.)* denotes a universal, non-dimensional function. However, it has been shown to be more convenient to work with the time-averaged velocity gradient, because the velocity gradient determines both the viscous stress and the production of turbulence (Pope 2000). Thus,

$$\frac{d\,\bar{u}(z)}{d\,z} = \frac{u_*}{z}\,\phi(\frac{z\,u_*}{\nu}, \frac{z}{\delta}) \qquad \text{for } z/\delta << 1 \quad (14b)$$

In the inner region, Prandtl (L. Prandtl, 1875-1953) postulated that the mean velocity gradient is determined by the viscous scale and, thus,

$$\frac{d\,\bar{u}(z)}{d\,z} = \frac{u_*}{z}\,\phi(z^+) \qquad \text{for } z/\delta << 1 \quad (15)$$

with ϕ referring to an unknown function. Integrating (15) in the wall-normal direction,

$$u^+ = \frac{\bar{u}(z)}{u_*} = f_w(z^+) = \int_0^{z^+} \frac{1}{z'}\,\phi(z')\,dz' \qquad \text{for } z/\delta << 1 \quad (16)$$

As previously mentioned, flow features are *not* dictated by viscosity *above* the inner layer. Therefore, ϕ should not be dependent on δ_v, which *is* indeed a function of viscosity. Mathematically, this is stated as

$$\phi(z^+) = \frac{1}{\kappa} \qquad \text{for } z/\delta << 1 \text{ and } z^+ >> 1 \quad (17)$$

where κ is von Kármán constant (T. von Kármán, 1881-1963). This leads to:

$$\frac{d\,\bar{u}(z)}{d\,z} = \frac{u_*}{z\,\kappa} \qquad \text{for } z/\delta << 1 \qquad (18)$$

which, upon integration gives:

$$\frac{\bar{u}(z)}{u_*} = \frac{1}{\kappa} \ln z^+ + C_1 \qquad (19)$$

Equation (19) is known as the logarithmic *law of the wall*, log law, or semi-logarithmic velocity law for a smooth boundary, developed by von Kármán. It is generally accepted that κ is about 0.4 (Davidson 2005), and the constant of integration is C_1 = 5.2 to 5.5. Comparison with experimental data indicates that the predictive capability of the law of the wall is excellent for $z^+ > 30$ and $z/\delta < 0.2$ (see Figure 4(b)). This law has been found to provide accurate predictions for many shear flows (Pope 2000).

Using a Taylor series expansion, it can be shown that, for small values of z^+, $f_w(z^+) = z^+ + O(z^{+2})$, where $O(h)$ indicates the quantity of big order h (Pope 2000). From highly-resolved simulation results of Kim et al. (1987), it is possible to conclude that $f_w(z^+) = z^+$ for $z^+ < 5$ -- the viscous sub-layer region (Pope 2000). This leads to a linear distribution of the velocity along the wall-normal direction in this region (or curved in a semi-logarithmic plot; see Figure 4(b)).

When the flow behavior is fully rough, the roughness height becomes a parameter that can *not* be disregarded. A combined expression that describes smooth, transitional and fully-rough behaviors is as follows (White 1974):

$$\frac{\bar{u}(z)}{u_*} = \frac{1}{\kappa} \ln z^+ + 5.5 - \frac{1}{\kappa} \ln(1 + 0.3\,k^+) \qquad (20)$$

where $k^+ = k\,u_*/\nu$. Equation (20) can be immediately interpreted as the result of subtracting a "roughness function" on k^+ from Equation (19). Thus, the velocity distribution for a rough boundary has the same slope as the velocity distribution for a smooth one, but it is shifted

downwards (White 1974, page 489). An equation that describes solely the fully-rough regime is as follows:

$$\frac{\bar{u}(z)}{u_*} = \frac{1}{\kappa} \ln \frac{z}{k} + 8.5 \qquad (21)$$

Additional information regarding laws of the time-averaged velocity in open channels and pipes can be found in Schlichting (1968), White (1974), Yen (1992a), Pope (2000), and Davidson (2005, page 130). Some authors have recently questioned the conceptual rigor, accuracy, and universality of the logarithmic law of the wall, and have suggested power laws for the flow velocity instead (Schlichting 1968; Yen 1992a; Barenblatt et al. 2000). Others, have focused on the lack of universality of the logarithmic law of the wall with constant parameters, but have stated its standing as a "robust and efficient workhorse for engineering applications" (Buschmann and Gad-el-Hak 2003, 2007, 2009).

Integrating Equations (19) to (21), or other similar ones, gives the cross-sectionally averaged velocity, *U*. These results can then be compared to the empirical formulations of flow resistance of Section II.1 (Chen 1992). In fact, integrating Equation (21) from *k* to the water depth, *H*, results in an equation which provides close results to Manning's power law. The resulting equation is: $U = \frac{u_*}{\kappa} \ln\left(\frac{11\,H}{k}\right)$, known as Keulegan's resistance relation for rough flow (García 1999; Bombardelli 2010). This outcome offers an interesting and noteworthy verification of the legitimacy of Manning's empirical expression for fully-rough flows.

Integrating Equation (19), and applying (6), it is possible to obtain, after small corrections:

$$\frac{1}{\sqrt{f}} = 2 \log_{10}\left(\sqrt{f}\ \mathrm{Re}\right) - 0.8 \qquad (22)$$

Equation (22) is known as the Prandtl's law for smooth pipes, and gives an implicit expression for the friction factor *f* as a function of the Reynolds number. Results obtained with Equation (22) agree with experimental data for a large range of values of the Reynolds number. Results obtained with (22) are also in close agreement with values obtained with the following empirical equation proposed by Blasius in 1911 (P. R. H. Blasius, 1883-1970), up to Reynolds numbers of approximately 100,000 (Schlichting 1968, page 573):

$$f = 0.3164\ \mathrm{Re}^{-1/4} \qquad (23)$$

beyond which the Blasius equation deviates from the data.

In a paper published in 1937, Colebrook and White proposed a formula for the friction factor, *f*, characterizing the flow in the smooth, transitional and fully-rough regimes. This formula gives *f* as a function of the relative roughness, *k/D*, and the Reynolds number, Re, as follows:

$$\frac{1}{\sqrt{f}} = -2\log\left(\frac{k}{D}\frac{1}{3.7} + \frac{2.51}{\mathrm{Re}\sqrt{f}}\right) \qquad (24)$$

This is also an implicit equation. Swamee and Jain (1976) developed in turn an *explicit* equation for the friction factor, written as follows:

$$f = \frac{0.25}{\left[-\log\left(\frac{k}{D}\frac{1}{3.7} + \frac{5.76}{\mathrm{Re}^{0.9}}\right)\right]^2} \qquad (25)$$

II.2.3 Nikuradse, and Moody/Rouse diagrams for the friction factor of flow in pipes, and equivalent diagram for the friction factor of flow in open channels

One of the pioneering and weightier experimental contributions regarding flow resistance in pipes is that of Nikuradse. Nikuradse reported values of the friction factor in a wide range of pipe flow conditions, as a function of the Reynolds number and the relative roughness (Nikuradse 1933). In his distinctive and classic experiments, sand grains of *uniform* size (denoted as k_s), were glued to the walls of pipes (of radius R) in a dense, compact manner, covering a range of ratios k_s/R between 1/15 and 1/500. Using uniform, compact layers of sand grains proved to be crucial in obtaining a simple definition of the roughness height with just *one* parameter (i.e., there was no need for the specification of density or area distribution of the grains, which are factors usually overlooked in works regarding flow in commercial pipes). Figure 5 shows the experimental results of Nikuradse for laminar and turbulent flow. Six curves characterize the flow in the right-hand side of the diagram, for different k_s/R values. In that portion of the chart, the curves are horizontal, indicating that the Reynolds number does not exert influence on the friction factor. These curves denote fully-rough flow behavior and follow the so-called Strickler scaling, i.e., $f \sim (k_s / R)^{1/3}$, which can be obtained from Equations (6) and (10) (see also Gioia and Bombardelli 2002). (The symbol "~" means "scales with".) Beyond Re $\approx$ 3,000 ($\approx$ 3 in log-scale) within the turbulent regime, the experimental points show higher values of f as the Re increases, where the curves form a "bundle" followed by a "hump" (Gioia and Chakraborty 2006). After the "hump," the bundle curves down towards the regression for smooth flows (Blasius scaling, $f \sim \mathrm{Re}^{-1/4}$, Equation (23)). The diverse curves deviate from the smooth-flow curve forming a set of "bellies" (Gioia and Chakraborty 2006) which continue into the fully-rough behavior lines. This region of the diagram represents the transitional regime.

Further details about Nikuradse's experiments can be found in Schlichting (1968).

In an effort to characterize the resistance to flow in commercial pipes, Moody (1944) presented a plot of *empirical* relations for turbulent flows developed by Blasius (1913), Prandtl (1935), Colebrook (1939), and Colebrook and White (1937). The idea for such a diagram had been previously suggested by Rouse (H. Rouse, 1906-1996), although he used different variables plotted on each axis. The Moody/Rouse chart is reproduced as Figure 6. The transitional regime curves do not show the inflection portion (i.e., neither the "bellies," nor the "hump") seen in the Nikuradse's chart -- an intriguing feature. This discrepancy does not have a clear explanation.

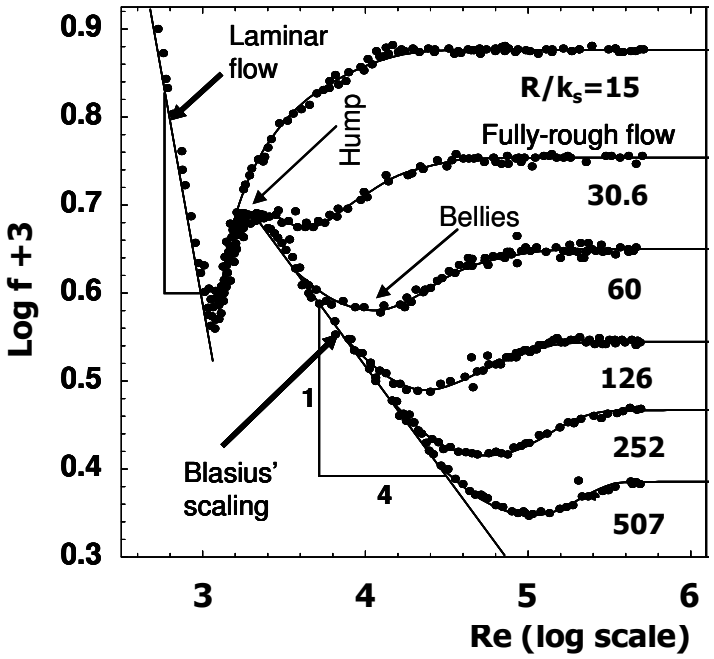

Figure 5. Nikuradse's diagram for circular pipes (adapted from Gioia and Chakraborty 2006). In this diagram, the roughness is k_s, obtained as the result of gluing sand grains to the pipe walls.

Colebrook and White (1937) argued that in commercial pipes with varying roughness heights, it is the largest roughness elements the ones responsible for the point of departure of the curves from the smooth line, while the point of collapse with the rough curves is determined by the smallest roughness elements (Langelandsvik et al. 2008).

Experimental results on the friction factor for non-circular pipes showed a dependence on shape of the cross section (Schlichting 1968, page 576). This dependence of the friction factor on the shape of the cross section also appears for open-channel flow.

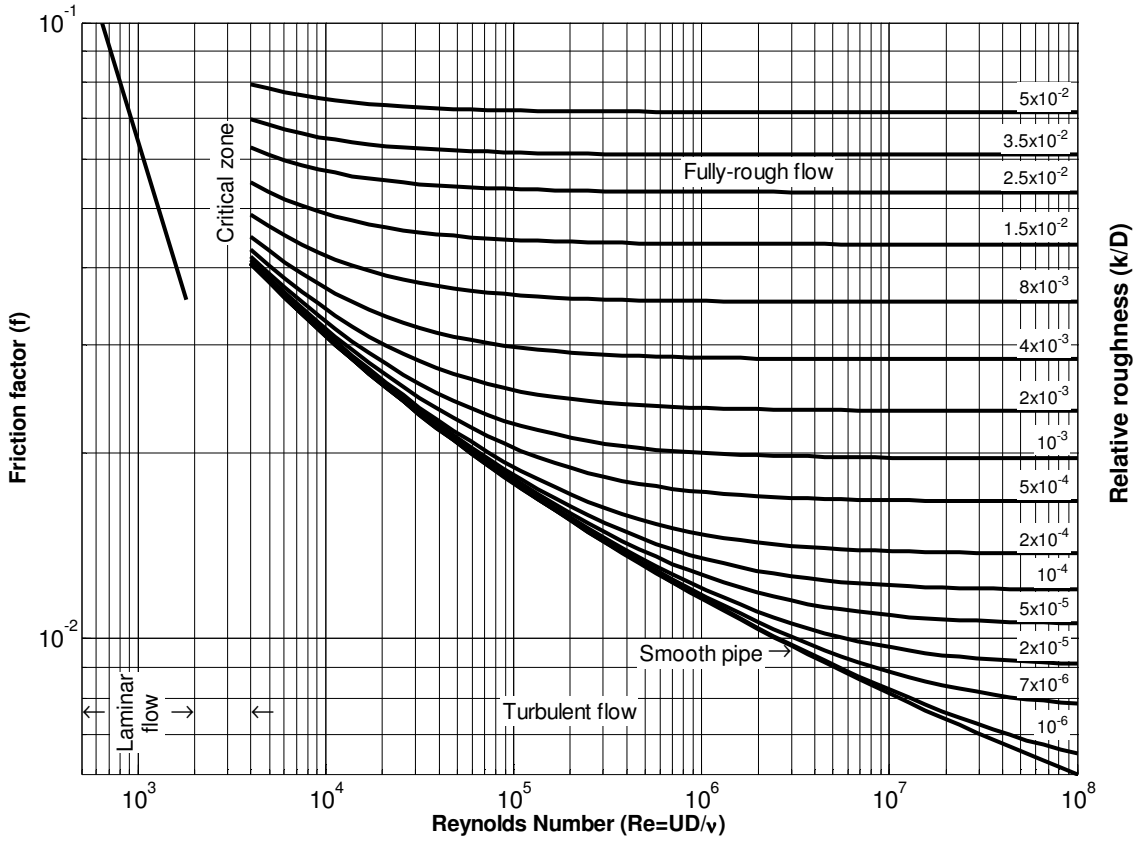

Figure 6. Moody/Rouse diagram for circular commercial pipes, obtained by plotting Equation (25) for the turbulent regime and $f = 64/\mathrm{Re}$ for the laminar regime.

Yen (1992a, 2002; B. C. Yen, 1935-2001) attempted to produce a diagram for the friction factor for *open-channel flow* for impervious rigid boundaries. To that end, he employed in abscissas the Reynolds number based on the hydraulic radius, Re_R, and included the few existing data on the subject, which were mainly obtained in the 1930s and 1960s. It could be argued that the presence of the free surface would affect the role of the relative roughness in the fully-rough

regime, but that role of the free surface is currently not completely understood.

Figure 7 shows a tentative diagram for open-channel flow (Yen 1992a, 2002). The chart shows that the *shape* of the channel is important both in the laminar regime and the fully rough region. Although all curves are represented by $f = K_L / \mathrm{Re}_R$ in the laminar region, the values of K_L range from 14.2 for an isosceles triangular channel, to 24 for a wide channel. For flow in a semi-circular channel, or a full pipe, $K_L = 16$. In the transitional and fully-rough regions, the available information is scarce. Yen (1992a, 2002) recommended using the following modified Colebrook-White equation for $\mathrm{Re}_R > 30{,}000$:

$$\frac{1}{\sqrt{f}} = -\, c_1 \log\left(\frac{k}{R_h} \frac{1}{c_2} + \frac{c_3}{4\ \mathrm{Re}_R\ \sqrt{f}} \right) \qquad (26)$$

with $c_1 = 2.0$, $c_2 = 14.83$, and $c_3 = 2.52$. Yen noted that the values of K_L and c_3 decrease for decreasing width to depth ratio, while c_2 increases and c_1 slightly increases. In addition, Yen showed that the curves for a wide open channel do not differ significantly from those corresponding to full pipes, for small values of the ratio *k/R*. However, he recommended further experiments to complete and validate the diagram.

II.3 Elements of the phenomenological theory of turbulence

Turbulent flow present in WDSs are characterized by a wide range of length scales. This is consistent with all turbulent flows found in nature that have a high Reynolds number. These length scales can be associated with "eddies" ("vortex blobs," Davidson 2005, page 131) varying from the largest flow length scales (L, determined by the size of the flow) to the smallest one, η_K, given by the Kolmogorov length scale (A. N. Kolmogorov, 1903-1987; see Davidson 2005, page 17; Pope 2000; Frisch 1995). Although eddies are difficult to define (see discussion in Davidson 2005, page 52, or Pope 2000, page 183), the scientific notion of eddies shares remarkable

similarities with the scales of flow in the famous sketches of Leonardo Da Vinci (1452-1519) of water falling into a pool (Davidson 2005, plate 3; Frisch 1995, cover). The Kolmogorov length scale is the length scale at which the turbulent fluctuations are dissipated into heat by viscosity (Davidson 2005). In pipe flow, the largest flow length scales are of the order of the pipe radius, and are determined by either the channel width or depth in open-channel flow (Gioia and Bombardelli 2002). The ratio of the large flow length scale and the Kolmogorov length scale can be shown to scale as the flow Reynolds number of the large scales to the ¾ power.

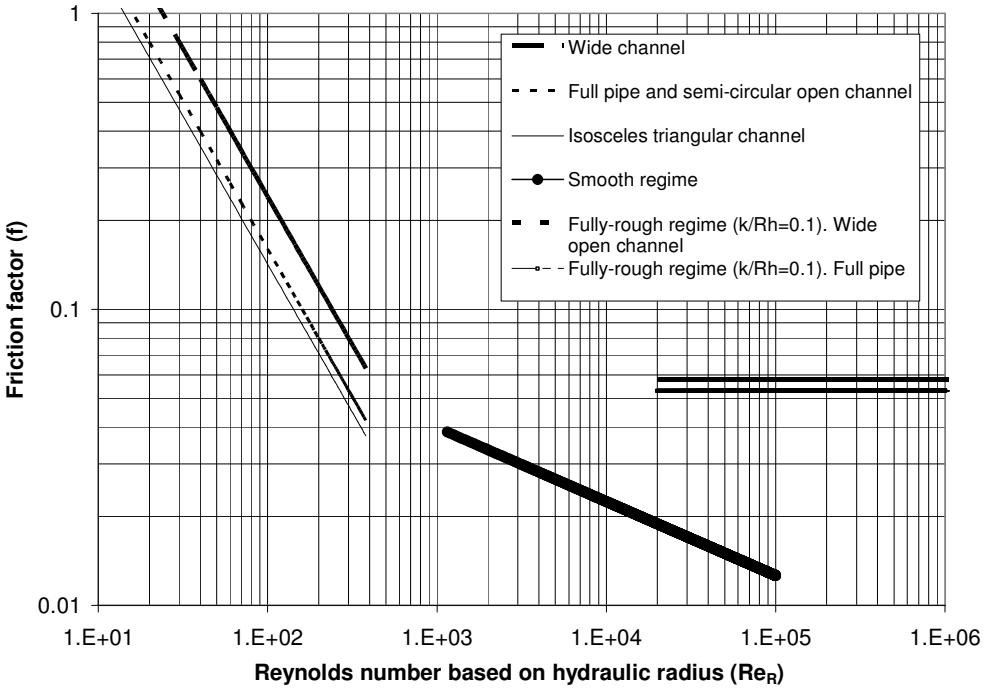

Figure 7. Diagram for the friction factor for open-channel flow, constructed based on information from Yen (1992a, 2002).

———————

Example 2 (on the length scales in a turbulent flow): For a pipe with a diameter of 0.4 m with a mean velocity of flowing water of 1 m/s, the ratio $L/\eta_K \sim \mathrm{Re}^{3/4} = (1\ \mathrm{m/s}\ 0.4\ \mathrm{m}/10^{-6}\ \mathrm{m^2/s})^{3/4} \approx$ 16,000. Usually, the values of η_K are of the order of fractions of millimeters.

———————

The intrinsic problem with the current analysis of turbulent flows is that there is no formal or general theory that is able to explain flow features under a wide range of situations. Most of the existing theories are valid for specific cases only, such as the theories for boundary layers, stratified flows, wall-bounded flows, etc. In spite of this state of affairs, there are two significant tools that can be used to address turbulent flows. These tools are based on the concept of *energy cascade* suggested by Richardson in 1922 (L. F. Richardson, 1881-1953; Pope 2000; Davidson 2005) and the Kolmogorov analysis for small scales (Kolmogorov 1991).

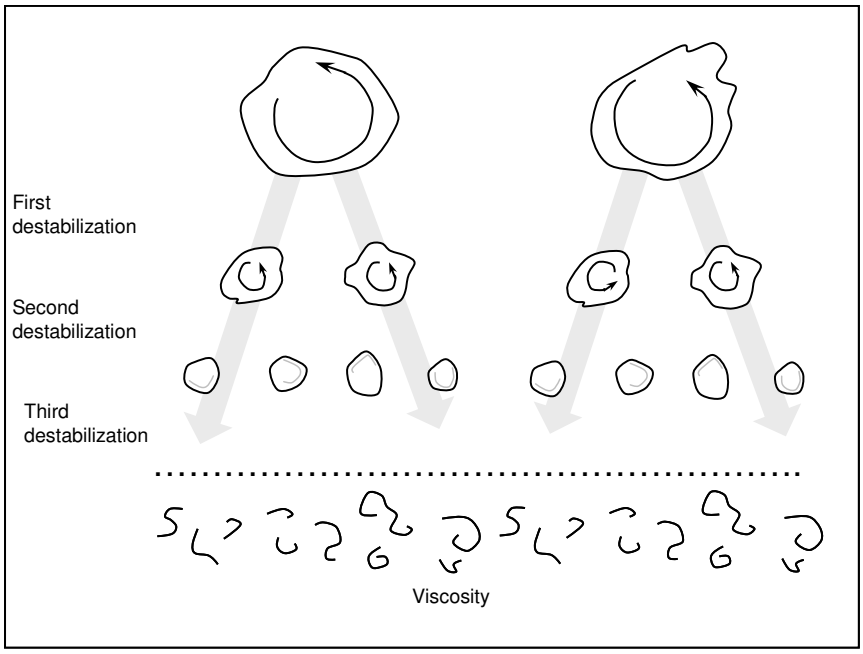

Figure 8. Schematic of the energy cascade. Adapted from Davidson (2005).

The concept of the energy cascade considers that the largest eddies in the flow suffer from inertial instabilities and that, consequently, they "break up" (i.e., loose identity), splitting their energy into two eddies of approximately half their original size during an overturn time. (The overturn time is defined as the lifespan of an eddy.) These resulting eddies also suffer from further instabilities, evolving into, and simultaneously transferring their energy to smaller eddies.

Interestingly, viscosity does not play any role in this transfer of energy (Davidson 2005). The rate at which the small scales receive energy from the large scales is equal to the rate at which the turbulent kinetic energy is dissipated (i.e., ε) in statistically steady turbulence. The instabilities of eddies and the transfer of energy continues until the size of the eddies becomes so small that viscosity becomes important and the energy is dissipated into heat at the Kolmogorov length scale. Figure 8 shows a schematic describing such a cascade.

The Kolmogorov theory for small scales states that these scales are *statistically isotropic* (i.e., the probability density function (PDF) of the velocity field is independent of the point in space considered (local homogeneity), and the PDF is invariant with respect to rotations and reflections of the coordinates axes; see Pope 2000, page 190) and have also a structure which is *statistically universal* (i.e., a structure which is valid for pipe flow, open-channel flow, boundary layers, wakes, etc.; Davidson 2005). The theory additionally states that for local isotropic turbulence, the statistical properties are a function of only the viscosity and the rate of transfer of energy via the cascade. This description of turbulent flows is summarized in Figure 9, which shows the scale ranges in a logarithmic scale. The dissipation range, close to the Kolmogorov length scale, where the turbulent fluctuations are dissipated into heat, extends up to a length scale l_{DI} of about 50-60 η_K (Pope 2000). On the opposite side of the spectrum, there is the energy-containing range, extending for length scales larger than l_{EI} (approximately, 1/6 L; Pope 2000). The small scales in Kolmogorov's analysis are smaller than l_{EI}. The zone between the energy-containing range and the dissipation range is called the *inertial sub-range*. These tools and ideas constitute the basis for the so-called *phenomenological theory of turbulence*. This theory rests on two main tenets that pertain to the transfer of turbulent kinetic energy: (1) The transfer of energy starts at the length scale of the largest eddies, and (2) the rate of energy transfer is

independent of viscosity. Under these tenets, the Taylor-Kolmogorov scaling states that:

$$\varepsilon \sim \frac{V^3}{L} \sim \frac{u_l^3}{l} \qquad (27)$$

where V indicates the velocity scale of the large eddies, and u_l refers to the velocity scale of a generic eddy located within the inertial sub-range (an eddy of size equal to l). This scaling was thought to apply in principle only to homogeneous and isotropic turbulence; however, recent research has provided evidence that the range of validity could be extended to flows that do not possess such features (see Section III.1).

Although this description of turbulence might be considered a rather simple "cartoon-like" approach, it has been shown to be very useful in providing physical insight into several practical cases (see Sections III.1 and III.2).

Another useful concept is the division of the flow field into a mean flow and a so-called "turbulent flow." In describing shear flows (a pipe flow for instance), Davidson (2005) stated: "the mean flow generates, maintains, and redistributes the turbulence, while the turbulence acts back on the mean flow, shaping the mean velocity distribution."

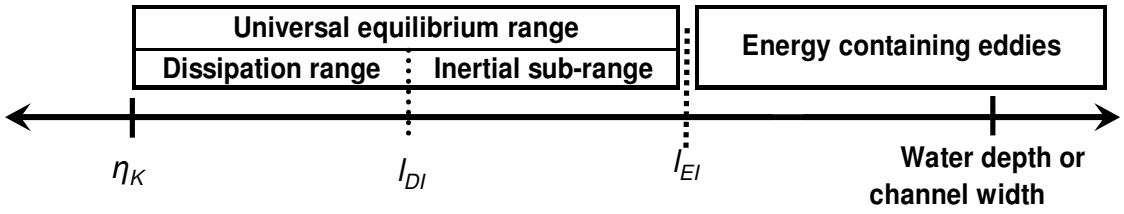

Figure 9. Schematic of the spectrum of scales in a turbulent flow. Adapted from Pope (2000).

II.4 The wave-number spectrum of energy in turbulent flows

The velocity spectrum tensor Φ_{ij} is defined for homogeneous turbulence as the Fourier

transform of the two-point correlation tensor, R_{ij} (Pope 2000):

$$\Phi_{ij}(\underline{\lambda}, t) = \frac{1}{(2\pi)^3} \iiint_{-\infty} e^{-i\,\underline{\lambda}\cdot\underline{r}}\; R_{ij}(\underline{r}, t)\; d\underline{r} \qquad (28)$$

$$R_{ij}(\underline{r}, t) = \iiint_{-\infty} e^{i\,\underline{\lambda}\cdot\underline{r}}\; \Phi_{ij}(\underline{\lambda}, t)\; d\underline{\lambda} \qquad (29)$$

where $\underline{\lambda}$ is the wavenumber vector, i and j are indices of the components of the tensor, and $\underline{r}$ is the distance vector; in turn, underlines indicate vectors. In Equations (28) and (29), $\underline{dr}$ and $\underline{d\lambda}$ represent the differentials in the three directions of the coordinate system. At $\underline{r} = \underline{0}$,

$$R_{ij}(0, t) = \iiint_{-\infty} \Phi_{ij}(\underline{\lambda}, t)\; d\underline{\lambda} = \overline{u_i'\, u_j'} \qquad (30)$$

Equation (30) relates the velocity spectrum in terms of the covariance $\overline{u_i'\, u_j'}$ (see Pope 2000, page 78). In the definitions (28) to (30), the variable indicating position, $\underline{x}$, has been removed because the turbulence field has been assumed to be homogeneous.

In addition to the tensorial expression, a simpler scalar version of the velocity spectrum can be defined. This is called the *energy spectrum function*, which removes all information on direction, as follows:

$$E(\|\underline{\lambda}\|) = \oint \frac{1}{2}\, \Phi_{ii}(\underline{\lambda})\; dS(\|\underline{\lambda}\|) \qquad (31)$$

Here $\|\underline{\lambda}\|$ indicates the modulus of the wavenumber vector, and $S(\|\underline{\lambda}\|)$ denotes the sphere in the wavenumber space with radius $\|\underline{\lambda}\|$ centered at $\underline{x} = \underline{0}$. It can be shown that (Pope 2000):

$$K = \int_0^{\infty} E(\|\underline{\lambda}\|)\; d\|\underline{\lambda}\| \qquad (32)$$

where K (= $\frac{1}{2}\; \overline{u_i'\, u_i'}$) is the flow turbulent kinetic energy (TKE). Several model spectra have

been proposed. One example of such models is:

$$E(\|\underline{\lambda}\|) = C_s\ \varepsilon^{2/3}\ \|\underline{\lambda}\|^{-5/3}\ f_L(\|\underline{\lambda}\|\ L)\ f_\eta(\|\underline{\lambda}\|\ \eta_K) \qquad (33)$$

where f_L is a dimensionless function dictating the shape of the energy-containing range, f_η is associated with the shape of the dissipation range, and C_s is a constant of proportionality. The function f_L becomes important when the product $\|\underline{\lambda}\|\ L$ is large, and f_η becomes large when the product $\|\underline{\lambda}\|\ \eta_K$ is small. In the inertial sub-range, $f_L = f_\eta = 1$, denoting the dominance of the factor $\|\underline{\lambda}\|^{-5/3}$. This last condition constitutes the well-known Kolmogorov spectrum, i.e., a spectrum in which the slope is -5/3. Experimental evidence obtained from different sources for diverse types of flow (wakes, pipes, grids, jets, etc.; Davidson 2005, page 226) indicates that *the scaled Kolmogorov spectrum is a universal function of the product of the wavenumber and the Kolmogorov length scale* (Saddoughi and Veeravalli 1994; Pope 2000).

III. ANALYSIS AND RESULTS

III.1 Manning's formula and the phenomenological theory of turbulence

Manning's formula is an empirical equation obtained as the result of mathematical regressions to several flow datasets that came from flumes and large rivers in North and South America, such as the Mississippi and Paraná Rivers (Dooge 1992; Yen 1992a). In a recent paper, Gioia and Bombardelli (2002) pioneered a derivation of Manning's formula starting from the phenomenological theory of turbulence, a result that connected for the first time two seemingly diverse fields: flow resistance formulations (Section II.1) and flow turbulence (Section II.3). To do this, Gioia and Bombardelli (2002) firstly applied the momentum balance, i.e., they equaled

the component of the weight in the direction of motion, to the force resisting the flow at the boundary in a uniform flow. They then scaled the shear stress effecting the transfer of momentum at the wall as the product of the tangential and normal velocities to a wetted surface tangent to the peaks of the roughness elements, and the density of water (Figure 10):

$$\tau \sim \rho\, v_n\, v_t \qquad (34).$$

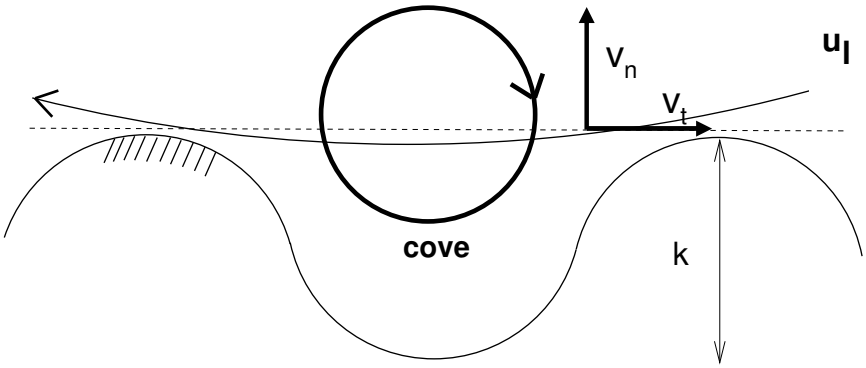

Figure 10. Schematic of the transfer of momentum by eddies at the wall. Adapted from Gioia and Bombardelli (2002); Bombardelli and Gioia (2005, 2006) and Gioia and Chakraborty (2006).

While the normal velocity was found to scale with the characteristic velocity of the eddies of size k (the size of the roughness elements), u_k, the tangent velocity was found to scale with the cross-sectionally averaged velocity U, leading to:

$$u_k\, U \sim R_h\, g\, S \qquad (35)$$

Next, Gioia and Bombardelli (2002) related u_k and U by making use of Equation (27), and assumed that eddies of size k located between roughness elements pertain to the inertial sub-range (Figure 10). This gives:

$$u_k \sim U \left(\frac{k}{R_h} \right)^{1/3} \qquad (36).$$

It is worth mentioning that the scaling embedded in the above equation implicitly assumes that the Taylor-Kolmogorov scaling is valid also for flows that are essentially non-homogeneous and

non-isotropic, such as wall-bounded flows. Recent research supports the assumption, including Knight and Sirovich (1990) and Lundgren (2002). Knight and Sirovich (1990) used the "empirical eigenvalue approach" to extend the Kolmogorov spectrum to conditions in which translational invariance (homogeneity) nor isotropy hold. They validated the results with data obtained from highly-resolved simulations (channel flow, Bénard convection), which show the appearance of an inertial sub-range. Lundgren (2002) employed matching asymptotic expansions to obtain the Kolmogorov two-thirds law (Pope 2000), relating the Kolmogorov theory and the Navier-Stokes equations. In 2003, Lundgren extended his theory to derive the inertial sub-range without imposing homogeneity and/or isotropy. Replacing Equation (36) in (35) gives:

$$U \sim \left(\frac{R_h}{k}\right)^{1/6} \sqrt{R_h \; g \; S} \qquad (37).$$

When Strickler's regression (Equation (10)) is applied to Equation (37), the standard form of Manning's formula (Equation (1)) is recovered.

Very interestingly, when $k \to \eta_K$ (the Kolmogorov length scale), Equation (37) gives:

$$U \sim \mathrm{Re}_R^{1/8} \sqrt{R_h \; g \; S} \qquad (38),$$

where Re_R is the Reynolds number based on the hydraulic radius. Since $f = 8 \; R_h \; g \; S/U^2$, Equation (38) leads to the scaling by Blasius: $f \sim \mathrm{Re}_R^{-1/4}$ (Equation (23))! This finding allows for the connection of well-known but seemingly unrelated scalings: Blasius', Kolmorogov's and Manning's (Gioia and Bombardelli 2002).

Gioia et al. (2006) employed similar reasoning based on the scaling of eddies to address the issue of intermittency in turbulence, and Bombardelli and Gioia (2005, 2006) and Gioia and Bombardelli (2005) used the same concepts to study the scour due to jets in pools.

III.2 Nikuradse's diagram, the spectrum, and the phenomenological theory of turbulence

Gioia and Chakraborty (2006) developed a theoretical/mathematical model that advanced the understanding of the physical mechanisms embedded in Nikuradse's chart. The model starts with the following expression for the velocity of eddies of size s, u_s (Pope 2000):

$$u_s^2 = \int_0^s E(\|\underline{\lambda}\|)\, \|\underline{\lambda}\|^{-2}\, d\|\underline{\lambda}\| \qquad (39)$$

where $E(\|\underline{\lambda}\|)$ denotes the turbulence spectrum, including the two correction functions for the energy-containing and the dissipation range (Equation (33) in Section II.4). Using the Taylor-Kolmogorov scaling (Equation (27)), and the scaling for the shear stress developed in the previous section (Equation (34)), Gioia and Chakraborty were able to obtain the following integral expression:

$$f = \Gamma \left[\int_0^{s/R} \Lambda^{-1/3}\, f_\eta(b\, \mathrm{Re}^{-3/4}/\Lambda)\, f_L(\Lambda)\, d\Lambda \right]^{1/2} \qquad (40)$$

where $\Lambda \equiv \|\underline{\lambda}\|/R$, and Γ and b are constants. Also, Re is the Reynolds number based on the pipe radius, and f_L and f_η are the dimensionless functions representing the shape of the ranges of energy-containing eddies and of dissipation, respectively (Section II.4). Equation (40) is an explicit function of Re and the relative roughness, *k/R*, of the pipe, because *s/R* is a function of *k/R* (Gioia and Chakraborty 2006). When evaluated numerically with the help of certain values of the constants, the integral expression developed by Gioia and Chakraborty provides an impressive *qualitative* agreement with Nikuradse's data, including all aspects of Nikuradse's chart (i.e., the "bundle" of curves, the "bellies," Blasius scaling, and the Strickler scaling) described in Section II.3 (see Figure 11). The theoretical model allows the chart to be interpreted as a manifestation of the transfer of momentum close to the wall by eddies located in the (i) energetic, (ii) dissipative, and (iii) inertial ranges (Figure 12). At the low values of the Reynolds

number in the turbulent regime of Figure 6 (of the order of 3,000), the momentum transfer is dominated by the large (energetic) eddies, which possess a velocity on the order of *U*, i.e., a velocity which scales with Re. This is the reason why the friction factor grows with growing values of the Reynolds number between Re = 3,000 and 3,500 (approximately). After the peak of the "hump," the curves plunge into the Blasius scaling (Figures 6 and 11), indicating that the momentum transfer is dominated by scales on the order of the Kolmogorov length scale, which is much larger than the roughness height for the smooth regime. Since the Kolmogorov length scale scales with the inverse of the Reynolds number to the 3/4 power, higher values of the Re lead to smaller eddy sizes and, consequently, the friction factor diminishes within the dissipative range. For larger values of the roughness height, the curves decrease to a lesser extent and start to deviate from Blasius' scaling. This behavior forms the "bellies" seen in Figures 6 and 11. As the Re increases, the roughness height becomes larger than the Kolmogorov length scale and, thus, the roughness height becomes more important in the transfer of momentum. Finally, when the inertial range is well established, the momentum transfer is effected by eddies of the size *k*, leading to Strickler's scaling, as predicted previously by Gioia and Bombardelli (2002).

Calzetta (2009) discussed Gioia and Chakraborty's (2006) model by using a different spectrum -- Heisenberg's spectrum. He found that his results fitted Nikuradse's data well. This demonstrates that the main features of the diagram are independent of the spectrum model employed.

Langelandsvik et al. (2008) reviewed the laws that describe the friction factor of commercial pipes. This was done using data obtained at unique facilities in the Department of Mechanical and Aerospace Engineering at Princeton University. They reported that Gioia extended Gioia and Chakraborty's 2006 theoretical model to consider two roughness heights that

differ in several orders of magnitude. This modified theoretical model predicts a monotonic curve for the friction factor with an abrupt transition from smooth to fully rough (Langelandsvik et al. 2008). Since the roughness heights in commercial steel pipes do not follow such a distribution, it is hard to extrapolate Gioia's theoretical model.

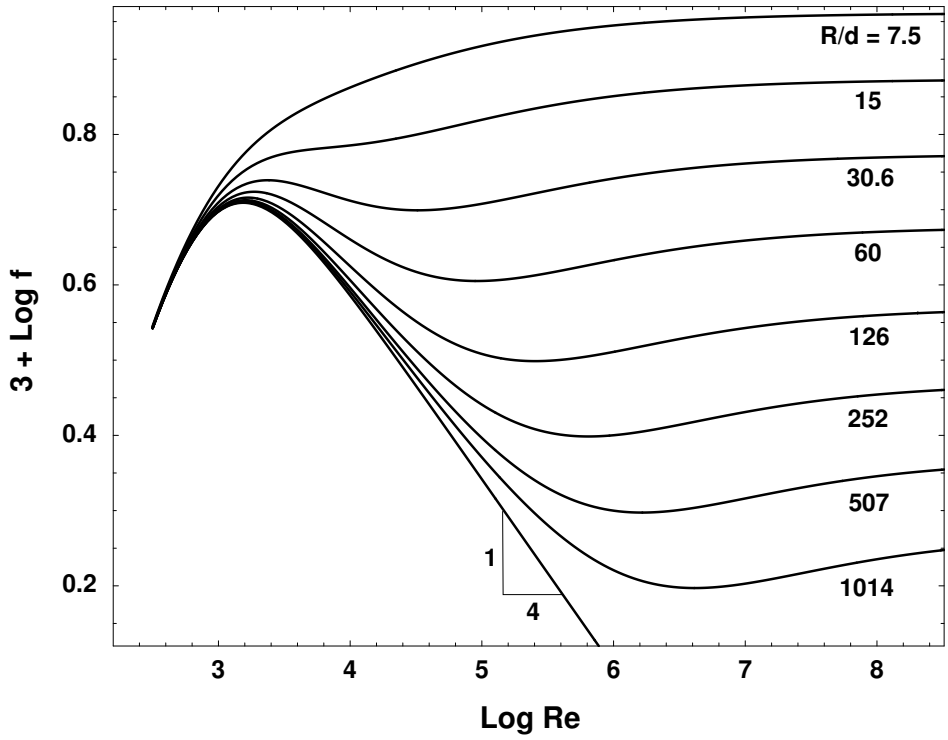

Figure 11. Numerical results of model by Gioia and Chakraborty (2006) obtained by performing the integral of Equation (40). In the diagram, *d* indicates the roughness height, *k*.

III.3 Range of validity of formulations for flow resistance

Equation (6) relates the resistance/conveyance coefficients associated with the different formulas. The details of the equivalence embedded is important to consider, because the diverse formulations have different ranges of applicability. Manning's equation (and the dimensionally homogeneous Manning's equation) should be used for fully-rough flows, which is the range for which there are theoretical derivations through integration of the velocity profile (Keulegan's relation; Section II.2) and through the phenomenological theory of turbulence (Section III.1).

Chèzy equation should also be used in the fully-rough regime. The Hazen-Williams formula's restricted range of applicability was confirmed by Bombardelli and García (2003). Analyzing the original dataset used by Williams and Hazen (1920), they determined that this range of applicability is limited to flows of Reynolds numbers between 10^4 and 2 x 10^6.

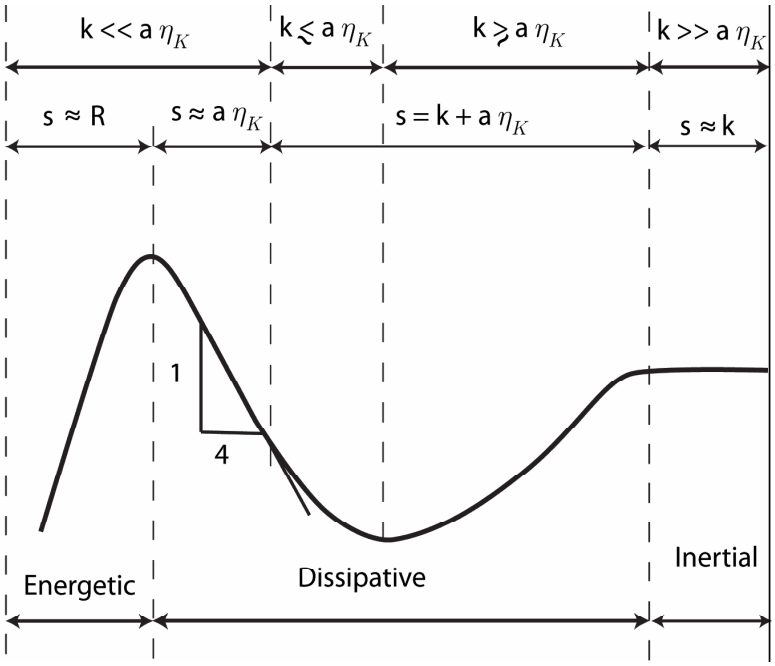

Figure 12. Schematic of the momentum transfer at the wall according to the eddies effecting the transfer (adapted from Gioia and Chakraborty 2006). *a* is a constant of proportionality.

Formulations which relate roughness heights with resistance/conveyance coefficients (such as Equations (10) and (11), for instance) should also be used with care. Bombardelli and García (2003) compared outcomes from Equation (10) against those using (6) and (25). They concluded that Equation (10) gives accurate results only when Manning's *n* is smaller than 0.02.

IV. ADDITIONAL TOPICS OF WATER DISTRIBUTION SYSTEMS

Other important topics associated with WDSs include: a) The selection of an adequate pumping capacity for a given WDS; b) hydraulic transients in pipe networks (pressurized flows); c) water

quality in pipe and open-channel flow; d) flow through gates; e) design of water towers; f) design of drop shafts; etc. Information on these and other topics of WDSs can be found in Mays (2005); Larock et al. (2008); Jeppson (1977); Watters (1984); Fischer et al. (1979). Some recent literature on WDSs has been devoted to the description and analysis of software packages used for the computation of flow and water quality in piping systems. One of such software packages is EPANET, developed by the Environmental Protection Agency (see http://www.epa.gov/nrmrl/wswrd/dw/epanet.html; and also Larock et al. 1999; Watters 1984). Another area of increasing interest in recent decades is given by issues associated with intentional spills of pollutants in large pipe systems (Mays 2004). Finally, the issue of proper WDS maintenance (i.e., cleaning of pipes and open channels; maintenance of tanks and buildings, etc.) is important and has received significant attention recently.

ACKNOWLEDGMENTS

The author thanks his students at UC Davis, Mr. James Kohne, Mr. Patricio Moreno, Mr. Dane Behrens, and Dr. Jamie Anderson from the California Department of Water Resources (DWR), for the comments provided on different versions of the manuscript. The chapter was completed thanks to funding provided by the California DWR (Dr. Anderson and Dr. Tara Smith as Program Managers), and the California Water Resources Control Board (Mr. Mark Gowdy as Program Manager). The author also thanks Prof. Harindra Joseph Fernando for his kind invitation to contribute to this book. This chapter is dedicated to the memory of Prof. Ben C. Yen, who was a pioneer in interpreting the design formulations for flow in pipes and open channels in light of the theory of fluid mechanics.

REFERENCES

Barenblatt, GI, Chorin, AJ, Prostokishin, VM. 2000. Self-similar intermediate structures in turbulent boundary layers at large Reynolds numbers. J. Fluid Mech., 410, 263-283.

Blasius, H. 1913. Das Ahnlichkeitsgesetz bei Reibungvorgangen in Flussigkeiten. Forschg. Arb. Ing., 135.

Bombardelli FA, García, MH. 2003. Hydraulic design of large-diameter pipes. J. Hydraulic Eng. ASCE, 129(11), 839-846.

Bombardelli, FA, Gioia, G. 2005. Towards a theoretical model of localized turbulent scouring. Proc. River, Coastal and Estuarine Morphodynamics (RCEM 2005, October 2005), Vol. 2,

pp. 931-936, G. Parker and M.H. García (Eds.), Taylor and Francis, London, 2006.
Bombardelli, FA, Gioia, G. 2006. Scouring of granular beds by jet-driven axisymmetric turbulent cauldrons. Phys. Fluids, 18, 088101.
Bombardelli, FA. 2010. Notes of the course "Urban Hydraulics and Hydrology," Department of Civil and Environmental Engineering, University of California, Davis.
Buschmann, MH, Gad-el-Hak, M. 2003. Generalized logarithmic law and its consequences. AIAA Journal, 41(1), 40-48.
Buschmann, MH, Gad-el-Hak, M. 2007. Recent developments in scaling wall-bounded flows. Progress in Aerospace Science, 42, 419-467.
Buschmann, MH, Gad-el-Hak, M. 2009. Evidence of non-logarithmic behavior of turbulence channel and pipe flow. AIAA Journal, 47(3), 535-541.
Calzetta, E. 2009. Friction factor for turbulent flow in rough pipes from Heisenberg's closure hypothesis. Phys. Rev. E, 79, 056311.
Chanson, H. 2002. An experimental study of Roman dropshaft hydraulics. J. Hydraulic Res., 40(1), 312, 320.
Chow, VT. 1959. Open-channel hydraulics. McGraw-Hill book company, Inc., USA.
Colebrook, CF. 1939. Turbulent flow in pipes, with particular reference to the transitional region between smooth and rough wall laws. J. Inst. Civil Engrs., 11, 133–156.
Colebrook, CF, White, CM. 1937. Experiments with fluid friction in roughened pipes. Proc. R. Soc. London A, 161, 367–378.
Davidson, PA. 2005. Turbulence. Oxford University Press, reprinted, New York, USA.
Diskin. MH. 1960. The limits of applicability of the Hazen-Williams formula. La Houille Blanche, 6, 720-723.
Dooge, JCI. 1992. The Manning formula in context. In *Channel flow resistance: Centennial of Manning's formula*, BC Yen (Ed.), Water Resources Publications, Littleton, CO, USA.
Fischer, HB, List, EJ, Koh, RCY, Imberger, J, Brooks, N. 1979. Mixing in inland and coastal waters. Academic Press, USA.
Frisch, U. 1995. Turbulence. Cambridge University Press, UK.
García, MH. 1999. Sedimentation and erosion hydraulics, in *Hydraulic Design Handbook*, LW Mays (Ed.), McGraw-Hill, USA.
Gioia G, Bombardelli FA. 2002. Scaling and similarity in rough channel flows. Phys. Rev. Lett., 88(1), 014501.
Gioia G, Bombardelli, FA. 2005. Localized turbulent flows on scouring granular beds. Phys. Rev. Lett., 95, 014501
Gioia G, Chakraborty, P. 2006. Turbulent friction in rough pipes and the energy spectrum of the phenomenological theory. Phys. Rev. Letters, 96, 044502.
Gioia G, Chakraborty, P, Bombardelli, FA. 2006. Rough-pipe flows and the existence of fully developed turbulence. Phys. Fluids, 18, 038107.
Jeppson, RW. 1977. Analysis of flow in pipe networks. Ann Arbor Science, USA.
Jiménez, J. (2004). Turbulent flows over rough walls. *Annual Review of Fluid Mechanics*, 36, 173-196.
Kim, J, Moin, P, Moser, R. 1987. Turbulence statistics in fully developed channel flow at low Reynolds numbers. J. Fluid Mech., 177, 133-166.
Knight, B., Sirovich, L. 1990. Kolmogorov inertial range for inhomogeneous turbulent flows. Phys. Rev. Lett., 65(11), 1356-1359.
Kolmogorov, AN. 1991. The local structure of turbulence in incompressible viscous fluid for

very large Reynolds numbers. Reprint, Proc. R. Soc. London A, 434, 9.
Kundu PK, Cohen IM. 2008. Fluid mechanics. Academic Press, New York, USA.
Langelandsvik, LI, Kunkel, GJ, Smits, AJ. 2008. Flow in a commercial steel pipe. J. Fluid Mech., 595, 323-339.
Larock BE, Jeppson, RW, Watters, GZ. 2008. Hydraulics of pipeline systems, CHIPS, USA.
Lundgren, TS. 2002. Kolmogorov two-thirds law by matched asymptotic expansion. Phys. Fluids, 14(2), 638-641,
Lundgren, TS. 2003. Kolmogorov turbulence by matched asymptotic expansion. Phys. Fluids, 15(4), 1074-1081,
Mays LW. 2004. Water supply systems security. McGraw-Hill Professional Engineering. McGraw-Hill, New York, USA.
Mays LW. 2005. Water resources engineering. John Wiley and Sons, Inc., New Jersey.
Mays LW. 2007. Water supply systems in arid and semi-arid regions during Antiquity: The use of cisterns. *Proc. Fifth Symposium on Environmental Hydraulics*, Tempe, Arizona, 205. (In CD.)
Mays LW. 2008. A very brief history of hydraulic technology during antiquity. Environmental Fluid Mechanics, 8, 471-484.
Masters, G. 1997. Introduction to environmental engineering and science. Prentice Hall, USA.
Nikuradse, A. 1933. Laws of flow in rough pipes. VDI Forschungshef, 361. Also NACA TM 1292, 1950.
Pope, SB. 2000. Turbulent flows. Cambridge University Press, UK.
Prandtl, L. 1935 The mechanics of viscous fluids. In *Aerodynamic Theory III* WF Durand (Ed.), 142; also Collected Works II, 819–845.
Saddoughi, SG, Veeravalli, SV. 1994. Local isotropy in turbulent boundary layers at high Reynolds number. J. Fluid Mechanics, 268, 333-372.
Schlichting H. 1968. Boundary-layer theory. McGraw-Hill book company, Sixth Edition, New York, USA.
Streeter, V, Wylie, EB, and Bedford, KW. 1998. Fluid mechanics. WCB McGraw-Hill, Ninth Edition, USA.
Strickler, A. 1981. Contribution to the question of a velocity formula and roughness data for streams, channels and close pipelines. Translation by T. Roesgen and W. R. Brownlie, Caltech, Pasadena.
Travis, QB, Mays, LW. 2007. Relationship between Hazen-William and Colebrook-White roughness values. J. Hydraulic Engineering, ASCE, 133(11), 1270-1273.
Watters, GZ. 1984. Analysis and control of unsteady flow in pipelines. Ann Arbor science book, Second Edition.
White, FM. 1974. Viscous fluid flow. McGraw-Hill, Inc., USA.
Williams, GS, and Hazen, A. 1920. Hydraulic tables. Third Edition. John Wiley and Sons, Inc. New York, USA.
Yen BC. 1992a. Hydraulic resistance in open channels. In *Channel flow resistance: Centennial of Manning's formula*, BC Yen (Ed.), Water Resources Publications, Littleton, CO, USA.
Yen BC. 1992b. Dimensionally homogeneous Manning's formula. J. Hydraulic Eng., ASCE, 118(9), 1326-1332.
Yen BC. 2002. Open channel flow resistance. J. Hydraulic Eng., ASCE, 128(1), 20-39.